

Moiré Topological Magnetism Twist-Engineered from 2D Spin Spirals

Zhonglin He,^{1,2} Kaiying Dou,¹ Wenhui Du,¹ Ying Dai,¹ Evgeny Y. Tsymbal,^{2,*} and Yandong Ma^{1,*}

¹*School of Physics, State Key Laboratory of Crystal Materials, Shandong University, Jinan 250100, China*

²*Department of Physics and Astronomy & Nebraska Center for Materials and Nanoscience, University of Nebraska, Lincoln, Nebraska 68588-0299, USA*

*Corresponding authors: tsymbal@unl.edu; yandong.ma@sdu.edu.cn

Abstract

Topological magnetism, characterized by topologically protected spin textures, offers rich physics and transformative prospects for spintronics. However, its stabilization typically demands external magnetic fields, preventing straightforward implementation. Here, we report a universal field-free approach for engineering 2D topologically-trivial spin spirals into topological magnetisms. This approach leverages twisted antiferromagnetic bilayers, where locked spin spirals in the two sublayers form spatially alternating ferromagnetic and antiferromagnetic domains upon twisting. These domains frustrate the uniform antiferromagnetic interlayer exchange, spontaneously stabilizing moiré topological magnetisms without external fields. Using first-principles and atomistic spin-model simulations, we validate this approach using bilayers NiCl₂ and NiBr₂, as representative examples. For twisted NiCl₂, we predict topological spin states tunable by the twist angle, including isolated and high-order antiferromagnetic bimerons. For twisted NiBr₂, strong frustration yields trivial triple-**q** spin spirals, which transform into moiré topological magnetism with the application of vertical compressive strain. Our findings demonstrate that topologically non-trivial spin textures can be engineered from their trivial counterparts, thus providing a new paradigm for topological spintronics.

Keywords: Moiré topological magnetism, first-principles calculations, frustrated magnetism, two-dimensional lattice, twist engineering

Introduction

Topological magnetism, characterizing topologically protected magnetic quasiparticles in real space, is one of the central topics in condensed matter physics and materials science [1-3]. It offers promising perspectives for information technology [4-6] and serves as a fertile platform for investigating fundamental phenomena such as the topological Hall effect [7], topological spin Hall effect [8], and skyrmion Hall effect [9]. The advent of two-dimensional (2D) magnetic materials [10-12] has further accelerated research in this field, attracting broad interest [13-16]. The emergence of topological magnetism in 2D systems stems from a delicate balance of competing magnetic interactions [17]. In this context, most 2D materials capable of hosting non-coplanar spin structures intrinsically stabilize trivial spin spirals rather than topological magnetism [18-20]. Current strategies to stabilize topological magnetism in such systems typically require additional external magnetic fields [21-23] posing significant constraints on practical device integration. There is thus an urgent need to explore new approaches for generating topological magnetism from 2D trivial spin spirals without external fields.

Moiré superlattices in 2D materials have served as a versatile platform for realizing new electronic phases (dubbed moiré electronics), as exemplified by the recent discoveries of topological insulators in twisted MoTe₂ [24,25] as well as unconventional superconductivity in twisted WSe₂ [26,27]. Inspired by moiré electronics, the magnetic counterpart, moiré magnets created by twisting magnetic atomic layers, is anticipated to host emergent magnetic phases distinct from those in natural 2D magnets [28,29]. Recent studies show that interlayer twist can induce non-coplanar spins in intrinsically collinear 2D magnetic systems [30,31] or modulate the physical properties of inherently 2D topological magnetic materials [32,33]. For instance, Antão et al. and Zhu et al. [34, 35] reported that in twisted bilayer, spatial variations in local point group symmetry of the moiré lattice can modulate the pre-existing topological properties [23, 36]. This raises the pivotal question of whether the twist can realize isolated moiré topological magnetisms in 2D systems originally hosting trivial spin spirals. Critically, no general strategy has yet been established to transform such trivial spirals into topologically protected moiré magnetism—

particularly without external fields.

In this letter, we introduce a universal approach for generating and controlling moiré topological magnetism in 2D systems originally hosting trivial spin spirals. The idea is to stack such systems into antiferromagnetic (AFM) bilayers. Upon twisting, local overlap of the locked spin spirals in the two sublayers forms spatially alternating ferromagnetic (FM) and AFM domains. These domains frustrate with the uniform AFM interlayer exchange interaction, spontaneously stabilizing moiré topological magnetism without external magnetic field. By performing first-principles calculations and atomistic spin model simulations, we demonstrate this mechanism for bilayer NiX_2 , where $X = \text{Cl}$ or Br . For NiCl_2 , we predict the emergence of topological spin states tunable by the twist angle, including isolated AFM bimerons, AFM merons, AFM antimerons, and high-order AFM bimerons. In NiBr_2 , strong frustration stabilizes trivial AFM triple- \mathbf{q} spirals, which evolves into topological magnetic textures under vertical compressive strain. These results establish a new paradigm for topological spintronics, where the topologically non-trivial spin textures can be twist-engineered from their trivial counterparts.

Results and Discussion

To engineer spin spirals in 2D materials, we first consider a single-layer (SL) magnetic lattice to set the stage. Non-coplanar spin structures arise primarily from two mechanisms: the Dzyaloshinskii-Moriya interaction (DMI) induced by broken inversion symmetry, and magnetic frustration, which may be intrinsic to the material. The spin structures of a SL lattice can be described by the model Hamiltonian

$$H_{\text{intra}} = -\sum_{\langle i,j \rangle} \mathbf{S}_i \mathbf{J}_{1,ij} \mathbf{S}_j - \sum_{\langle\langle i,j \rangle\rangle} J_2 \mathbf{S}_i \cdot \mathbf{S}_j - \sum_{\langle\langle\langle i,j \rangle\rangle\rangle} J_3 \mathbf{S}_i \cdot \mathbf{S}_j - \sum_{\langle i \rangle} K (\mathbf{S}_i \cdot \hat{\mathbf{z}})^2. \quad (1)$$

Here, \mathbf{S}_i denotes the spin vector at site i (position \mathbf{r}_i). $\hat{\mathbf{z}}$ is the unit vector perpendicular to the plane of 2D magnetic lattices. The nearest-neighbor (NN) exchange interaction tensor $\mathbf{J}_{1,ij}$ decomposes into

$$\mathbf{J}_{1,ij} = \mathbf{J}_{1,ij}^I + \mathbf{J}_{1,ij}^A + \mathbf{J}_{1,ij}^S, \quad (2)$$

comprising isotropic $\mathbf{J}_{1,ij}^I = \frac{1}{3}\text{Tr}(\mathbf{J}_{1,ij})\mathbf{I}$, antisymmetric DMI $\mathbf{J}_{1,ij}^A = \frac{1}{2}(\mathbf{J}_{1,ij} - \mathbf{J}_{1,ij}^T)$, and anisotropic symmetric $\mathbf{J}_{1,ij}^S = \frac{1}{2}(\mathbf{J}_{1,ij} + \mathbf{J}_{1,ij}^T) - \mathbf{J}_{1,ij}^I$ terms. We include exchange interactions up to the third nearest neighbor within the J_1 - J_2 - J_3 model and magnetic anisotropy K . With tuning these parameters, spin spirals with different wavevector $\mathbf{q} = (q_x, q_y)$ can be obtained. For simplicity, we consider single- \mathbf{q} spin spirals where we assume that $\mathbf{q} = (q_x, 0)$ is favored, so that

$$\mathbf{S}_i(\mathbf{r}_i) = \cos(\mathbf{q} \cdot \mathbf{r}_i + \phi)\hat{\mathbf{x}} + \sin(\mathbf{q} \cdot \mathbf{r}_i + \phi)\hat{\mathbf{z}}, \quad (3)$$

where $\hat{\mathbf{x}}$ is the unit vector along x and phase ϕ describes translation of spin spirals (**Fig. S1** [45]).

We then stack two such SL lattices together to construct a bilayer lattice. Initially neglecting interlayer interactions, the bilayer spin Hamiltonian is

$$H = \sum_{l=t,b} H_{\text{intra}}^l, \quad (4)$$

where $l = t, b$ labels the top and bottom layers, respectively. It is known that in a bilayer lattice, the interlayer exchange interaction is usually dominated with a uniform A-type AFM coupling regardless of the stacking pattern [37-39]. Following this principle, despite the absence of explicit interlayer coupling, we impose an inherent A-type AFM alignment. This results in AFM single- \mathbf{q} spin spirals with $\mathbf{q} = (q_x, 0)$ in the AA-stacked bilayer lattice, as illustrated in **Fig. S1** [45]. The spin vector can be expressed by $\mathbf{S}_i^l(\mathbf{r}_i^l) = \cos(\mathbf{q} \cdot \mathbf{r}_i^l + \phi^l)\hat{\mathbf{x}} + \sin(\mathbf{q} \cdot \mathbf{r}_i^l + \phi^l)\hat{\mathbf{z}}$, and ϕ^l is set to be 0 and 180° for the top and bottom layers, respectively.

Upon rotating the top layer with a twist angle θ , as illustrated in **Fig. 1(a)**, the local overlap between the locked spin spirals of the sublayers is cased, forming spatially alternating FM (red and blue areas) and AFM (purple areas) domains. The twisted top-layer spins now follow:

$$\mathbf{S}_i^t(\mathbf{r}_i^t) = \cos(\mathbf{q} \cdot \mathcal{R}(\theta)\mathbf{r}_i^t)\hat{\mathbf{x}} + \sin(\mathbf{q} \cdot \mathcal{R}(\theta)\mathbf{r}_i^t)\hat{\mathbf{z}}, \quad (5)$$

where $\mathcal{R}(\theta) = \begin{pmatrix} \cos \theta & -\sin \theta \\ \sin \theta & \cos \theta \end{pmatrix}$ is the in-plane rotation matrix. The bottom-layer spins remain

$$\mathbf{S}_i^b(\mathbf{r}_i^b) = -\cos(\mathbf{q} \cdot \mathbf{r}_i^b) \hat{\mathbf{x}} - \sin(\mathbf{q} \cdot \mathbf{r}_i^b) \hat{\mathbf{z}}. \quad (6)$$

Including interlayer interactions introduces an additional spin Hamiltonian term:

$$H_{\text{inter}} = -\sum_{\langle i,j \rangle} J_{\perp}(\mathbf{r}_i^t - \mathbf{r}_j^b) \mathbf{S}_i^t \cdot \mathbf{S}_j^b = -\sum_{\langle i,j \rangle} J_{\perp}(\mathbf{r}_{ij}) \mathbf{S}_i^t \cdot \mathbf{S}_j^b, \quad (7)$$

where the distance-dependent interlayer coupling $J_{\perp}(\mathbf{r}_{ij}) = J_{\perp}(\mathbf{r}_i^t - \mathbf{r}_j^b) < 0$ enforces uniform AFM interlayer coupling. Based on the interlayer spin Hamiltonian and spin spirals in the two sublayers, we can obtain the interlayer exchange energy (see Sec. II of Supplemental Material [45]). **Fig. 1(b)** displays the interlayer exchange energy versus position along the interdomain midline A-B [see **Fig. 1(a)**], revealing characteristic oscillations that energetically suppress FM domains. Crucially, this spatial alternation between FM and AFM domains frustrates the uniform AFM interlayer coupling. Since topological magnetic quasiparticles typically originate from competing magnetic interactions, such frustration can enable the spontaneous stabilization of moiré topological magnetism (i.e., emergent topological magnetic quasiparticles within moiré lattices), offering a novel pathway to engineer topological magnetism from trivial spin spirals in 2D systems. Additionally, this scenario also applies to 2D materials with multi- \mathbf{q} spin spirals.

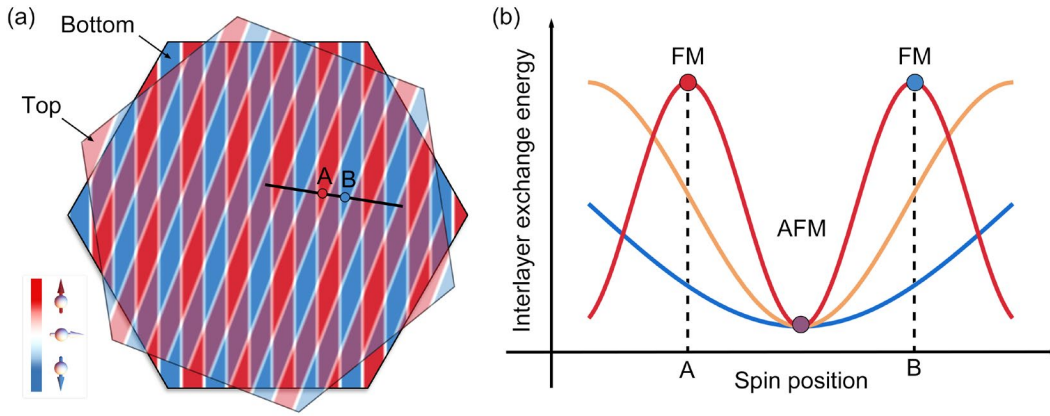


Fig. 1. (a) Schematic illustration of the spin spirals in twisted AFM bilayer in the absence of interlayer coupling. Out-of-plane spin components are denoted by colors. (b) Interlayer exchange

energy versus spin position along the interdomain midline A-B, as indicated in (a). Blue, orange and red lines in (b) represent interlayer exchange energies under twist angles of $\theta = 1.960^\circ$, 4.040° and 9.430° , respectively.

Two candidate materials to validate our proposed approach are NiX_2 ($X = \text{Cl}, \text{Br}$). SL NiX_2 crystallizes in a triangular lattice (space group $P\bar{3}m1$; **Fig. S2** [45]), with lattice parameters a_0 listed in **Table S1**, agreeing well with the previous work [23]. The electronic configuration of isolated Ni atom is $3d^84s^2$. By donating two electrons to X ligands, Ni adopts a +2 oxidation state in NiX_2 . Under an octahedral crystal field, the d orbitals of Ni split into t_{2g} and e_g manifolds. The Ni atom exhibits an electric configuration of $t_{2g}^6e_g^2$, which is expected to produce the magnetic moment of $2 \mu_B$. As anticipated, our calculations reveal that monolayer NiX_2 favors a spin-polarized state with a magnetic moment of $2 \mu_B$ per unit cell, primarily localized at Ni atoms.

Next, we perform Density Functional Theory (DFT) calculations to investigate the magnetic interactions in SL NiX_2 according to **Eq. (1)**. The four-state method is introduced to obtain exchange interactions J and magnetic anisotropy K (see Sec. III of Supplemental Material [45]). As listed in **Table. S1**, SL NiX_2 exhibits FM NN exchange interaction ($J_1 > 0$) and AFM third NN isotropic exchange interaction ($J_3 < 0$), while the FM next NN isotropic exchange interaction is negligible. This hierarchy stems from the super-exchange mediated by delocalized p states of X atoms [23,40]. We find that the ratio of J_3/J_1 is -0.33 and -0.49 for NiCl_2 and NiBr_2 , respectively, revealing the increasing exchange frustration across the ligand series. Due to inversion symmetry, DMI is forbidden in SL NiX_2 . The obtained negative values of K suggest that they exhibit in-plane magnetization. To explore the spin textures in SL NiX_2 , we perform atomistic spin model simulations based on the spin Hamiltonian of **Eq. (1, 2)** and the Landau-Lifshitz-Gilbert (LLG)-Heun method implemented in the VAMPIRE package (see Sec. I of Supplemental Material [45]). As shown in **Fig. S3** [45], both systems exhibit trivial spin-spiral textures. Such trivial spin spirals are further confirmed by the spin structure factor [41]

$$S(\mathbf{q}) = (1/N^2) \sum_{\mu=x,y,z} \left\langle \left| \sum_i \mathbf{S}_i \cdot \hat{\mathbf{r}}_\mu \exp(-i\mathbf{q} \cdot \mathbf{r}_i) \right|^2 \right\rangle, \quad (8)$$

where N and i represent the number of spins and imaginary unit, respectively. Whereas SL NiCl₂ exhibits multi- \mathbf{q} spin spirals, SL NiBr₂ favors single- \mathbf{q} spin spirals (**Fig. S3** [45]). This distinction is due to their different exchange frustration strengths, namely J_3/J_1 is larger for NiBr₂ than for NiCl₂.

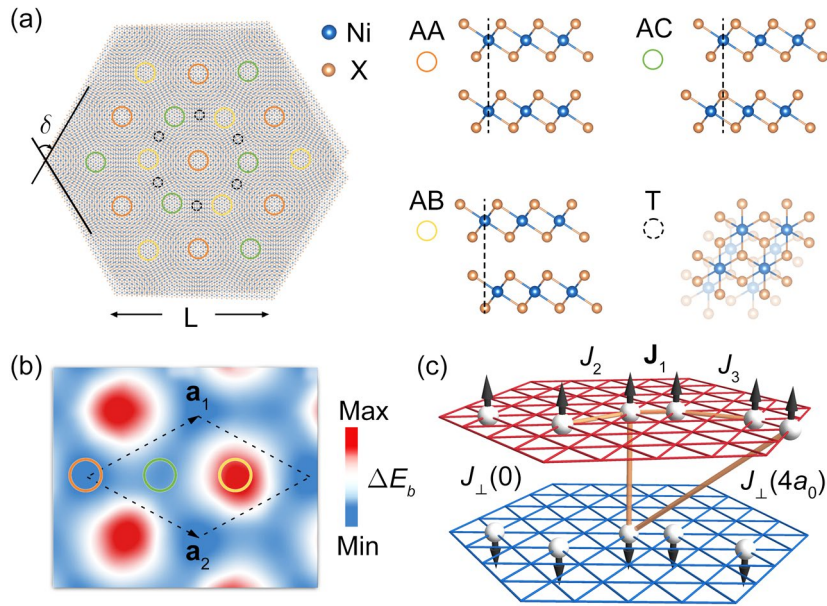


Fig. 2. (a) Crystal structure of twisted bilayer NiX₂ with twist angle $\theta = \delta - 60^\circ = 1.096^\circ$. Right panel in (a) shows the crystal structures of AA-, AB-, AC- and T-stacked patterns which are denoted by orange, yellow, green and black circles, respectively, in left panel. Blue and orange balls represent Ni and X atoms, respectively. (b) Interlayer coupling energy ΔE_b of NiCl₂ as a function of an interlayer shift \mathbf{r} . (c) Schematic diagram of intralayer and interlayer magnetic interactions in twisted bilayer NiX₂.

Building on the SL magnetic behavior, we extend our analysis to bilayer NiX₂ with interlayer exchange coupling quantified by interlayer coupling energy ΔE_b , which is defined by

the energy difference $\Delta E_b(\mathbf{r}) = E_{\text{FM}}(\mathbf{r}) - E_{\text{AFM}}(\mathbf{r})$ for lateral shifts $\mathbf{r} = \eta\mathbf{a}_1 + \nu\mathbf{a}_2$ (\mathbf{a}_1 and \mathbf{a}_2 are the lattice vectors). Computations of $\Delta E(\mathbf{r})$ on a 6×6 grids (validated against denser 9×9 and 11×11 grids; see **Fig. S4(c)** [45]) with $\eta, \nu = \left\{0, \frac{1}{6}, \dots, \frac{5}{6}\right\}$ reveal spatially similar AFM-favored coupling ($\Delta E_b > 0$) for both bilayer NiCl_2 and NiBr_2 [see **Fig. 2(b)**], though coupling strength varies with ligand (**Table S1** [45]). From this resulting ΔE_b , the interlayer exchange J_{\perp} of bilayer NiX_2 in **Eq. (7)** can be obtained, as detailed in Sec. III of Supplemental Material [45]). In contrast to the interlayer exchange that varies with stacking order, our DFT calculations indicate that the modifications to the intralayer interactions [isotropic exchange (J_1, J_2, J_3), magnetic anisotropy (K) and DMI ($\mathbf{J}_{1,ij}^A$)] imposed by interlayer coupling are negligible (**Table S2** [45]). We therefore construct the full bilayer spin Hamiltonian of **Eq. (1,4,7)** by combining the derived J_{\perp} with magnetic parameters of SL NiX_2 . Based on this parameterized spin Hamiltonian, we perform atomistic spin simulations to investigate the spin textures of AA-stacked bilayer NiX_2 , which is energetically favored over the AB and AC stacking (**Table S3** [45]). As shown in **Figs. S3(d-f)** [45], AFM single- \mathbf{q} spin-spiral features are observed in both cases. Crucially, bilayer NiCl_2 displays a longer spiral wavelength than NiBr_2 , consistent with its weaker exchange frustration. This reduced frustration biases the spins toward xy -plane, enhancing the in-plane spin components in NiCl_2 .

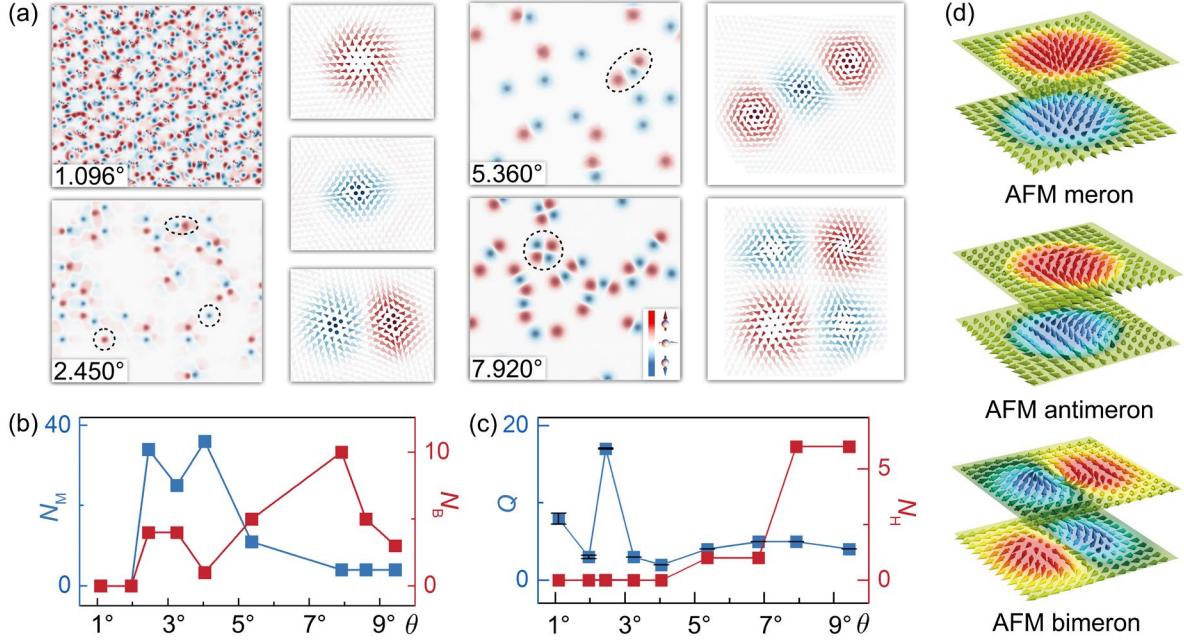


Fig. 3. (a) Spin textures of the top layer in twisted bilayer NiCl_2 at $\theta = 1.096^\circ$, 2.450° , 5.360° and 7.920° . Insets in (a) show the enlarged spin distributions of isolated merons, antimerons, bimerons, high-order merons and high-order bimerons. Out-of-plane spin components are denoted by colors and in-plane components are indicated by arrows. (b) Evolution of the total number of merons and antimerons, N_M , and bimerons, N_B , in twisted bilayer NiCl_2 as functions of θ . (c) Evolution of the total number of high-order merons and high-order bimerons, N_H , and Q_{up} , in twisted bilayer NiCl_2 as functions of θ . Error bars represent the deviation of Q from the nearest integer. (d) Schematic illustrations of spin distributions for AFM topological magnetisms in twisted bilayer NiCl_2 .

After establishing the AFM bilayer spin-spiral textures and uniform AFM interlayer coupling, we introduce an interlayer twist on the AA-stacked bilayer NiX_2 (defined as $\theta = 0$) to form a long-period moiré pattern. The twist angle $\theta = \frac{180^\circ}{\pi} \arccos \left[-\frac{1}{2} + \frac{3m(m-n)}{2(m^2 - mn + n^2)} \right]$ and

moiré periodicity $L = a_0 \sqrt{m^2 + n^2 + mn} = \frac{|m-n|a_0}{\sin(\theta_{m,n}/2)}$ are defined using a pair of coprime integers

(m, n) to ensure the commensurability of moiré lattice. For simplicity, n is fixed at 1 with m

variable. As **Fig. 2(a)** illustrates for $\theta = 1.096^\circ$, the resulting long-period moiré lattice exhibits spatially varying stacking orders, mapped onto the high-symmetry configurations AA, AB, AC, and T with interlayer shifts $\mathbf{r} = 0, \frac{\mathbf{a}_1 + \mathbf{a}_2}{3}, \frac{2(\mathbf{a}_1 + \mathbf{a}_2)}{3}, \frac{\mathbf{a}_2}{2}$, respectively. This spatial variation generates tens of thousands of nonequivalent magnetic interactions within a moiré unit cell, complicating the determination of magnetic properties.

Following prior works [29-31], we extend the bilayer spin Hamiltonian to twisted bilayer NiX_2 by adopting a widely employed approximation [40]: intralayer magnetic interactions are assumed identical to those in SL NiX_2 and spatially uniform throughout the moiré unit cell, while the moiré interlayer coupling energy ΔE_m is derived from ΔE_b using a sliding-mapping approach [**Fig. S4(b)**]. This mapped moiré interlayer coupling energy ΔE_m allows us to determine the interlayer exchange interactions J_\perp across the moiré lattice (see Sec. III of Supplemental Material [45]). With the first-principles parameterized moiré spin Hamiltonian established, we perform atomistic spin model simulations to explore the spin textures in twisted bilayer NiX_2 . It should be noted since we focus on the underlying physical mechanism, we restrict our analysis to the spin textures at $T = 0$ K. Given the reliability of our interlayer interaction approximation at small twist angle, we focus on the range of θ from 1.096° to 9.420° . **Figs. 3(a)** and **S5** [45] show the spin textures in the top layer of twisted bilayer NiCl_2 with different twist angle θ . At $\theta = 1.096^\circ$, the interplay between spin-spiral textures and moiré lattice gives rise to meron-antimeron loops, serving as an indication for topological magnetism [20,21]. Upon increasing θ , these loops gradually shrink and eventually vanish by $\theta = 2.450^\circ$, yielding isolated topological magnetisms on the top layer, including antimerons, merons and bimerons [**Fig. 3(a)**]. To quantify topological

nature of these spin textures, topological number $Q = \frac{1}{4\pi} \iint \mathbf{S}(\mathbf{r}) \cdot \left[\frac{\partial \mathbf{S}(\mathbf{r})}{\partial x} \times \frac{\partial \mathbf{S}(\mathbf{r})}{\partial y} \right] d^2 \mathbf{r}$ is calculated using the discrete form given in **Eq. S2**. **Fig. 3(c)** presents total topological number Q_{up} of the top layer. For $\theta < 2.450^\circ$, Q_{up} is non-integer, indicating that spin textures are not fully composed of topological magnetic quasiparticles. In contrast, with $\theta \geq 2.450^\circ$, the non-trivial

nature of these spin textures is confirmed by the non-vanishing and quantized Q_{up} . In this regime, the emergent topological magnetism is revealed in the appearance of a multitude of isolated merons and antimerons, with only a few bimerons observed. Accordingly, the total number of isolated merons and antimerons, N_M , rises steeply, in contrast to the weak increase of the total number of isolated bimerons, N_B [**Fig. 3(b)**]. As θ increases up to 5.360° , these isolated merons and antimerons begin to pair up. This pairing is evidenced by a sharp decline in N_M , accompanied by a surge in bimerons as well as the emergence of high-order merons [see **Figs. 3(b, c)**] [44]. With a further increase of θ , isolated bimerons also start to coalesce, leading to a reduction in N_B but the formation of high-order bimerons in the top layer. Turning from the top-layer viewpoint to the twisted bilayer as a whole, uniform interlayer AFM coupling stabilizes isolated AFM topological magnetisms [**Fig. 3(d)**] [8], with sublayers hosting spin textures with opposite topological numbers (**Fig. S6** [45]). This topological number compensation is expected to suppress the skyrmion Hall effect, a highly desirable feature for practical applications [43]. Despite the cancellation of the net topological number, unbalancing the layers provides a pathway for the detection and manipulation of these AFM topological quasiparticles [46]. Additionally, since lattice relaxation is known to occur in twisted bilayer NiI_2 [34, 35], we investigate its influence in twisted bilayer NiCl_2 and find that it has a minor impact on the emergence of topological magnetic quasiparticles (see Sec. VI in Supplementary Material). These results demonstrate the intriguing twist tunable moiré topological magnetism in twisted bilayer NiCl_2 .

To get insight into the twist tunability of the moiré topological magnetism in twisted bilayer NiCl_2 , we first explore the dependence of the spin textures on the stacking order. **Fig. S7(c)** [45] shows the spin textures of metastable AB- and AC-stacked bilayer NiCl_2 . Spin-spiral textures are preserved in AA- and AC-stacked bilayer NiCl_2 , while AB stacking favors an in-plane FM state. To pinpoint the origin of this dependence, evolutions of spin textures for bilayer NiCl_2 with the interlayer coupling energy ΔE_b are depicted in **Figs. S7(a, b)** [45]. Upon increasing the magnitude of ΔE_b , spin spirals continuously transform into in-plane FM states. These results

establish the interlayer coupling energy ΔE_b as the primary factor controlling spin textures in bilayer NiCl_2 . In twisted bilayer NiCl_2 , the stacking order varies across the moiré lattice, leading to a moiré modulation of interlayer coupling energy ΔE_b . This modulation partitions the moiré unit cell into local regions, denoted by AA, AB, and AC (inset in **Fig. S8** [45]). At small twist angle, local regions are relatively large, and spin textures are governed locally by ΔE_b . AA/AC regions favor meron–antimeron loops, whereas the AB region enforces in-plane textures. Further increasing the twist angle θ redistributes the sizes and arrangement of these ΔE -defined local regions (see **Fig. S8** [45]), thereby endowing moiré topological magnetism with twist tunability. More details are shown in Sec. IV of Supplemental Material [45].

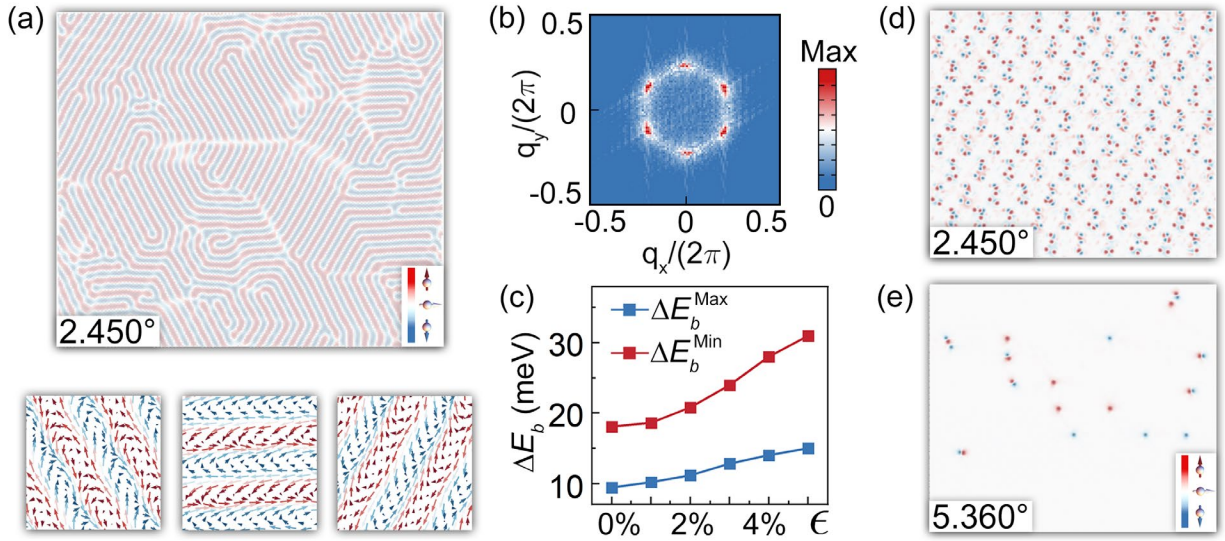


Fig. 4. (a) Spin textures of the top layer in twisted bilayer NiBr_2 at $\theta = 2.450^\circ$. Insets in (a) show the enlarged spin distributions of three types of spin spirals in triple- \mathbf{q} state. Out-of-plane spin components are denoted by colors and in-plane components are indicated by arrows. (b) Intensity plots of $S(\mathbf{q})$ in the extended Brillouin zone for spin textures in (a). (c) Evolution of interlayer coupling energy ΔE_b for bilayer NiBr_2 as a function of vertical compressive strain ϵ . Red and blue dot lines represent ΔE_b^{Max} and ΔE_b^{Min} , respectively. (d, e) Spin textures of the top layer in twisted bilayer NiBr_2 under $\epsilon = 5\%$ at $\theta = 2.450^\circ$ and 5.360° . Out-of-plane spin components are denoted

by color.

Unlike NiCl₂, the strong exchange frustration drives AFM spin-spiral textures in twisted bilayer NiBr₂ into a trivial AFM triple-**q** state, which is insensitive to twist angle θ (**Fig. S9** [45]). This triple-**q** state is composed of three degenerate spin spirals [insets in **Fig. 4(a)**], indicating trivial spin textures. Based on the above discussion, the interlayer coupling energy ΔE_b plays a crucial role in the emergence of topological magnetism. Since ΔE_b originates from interlayer interactions, it can be effectively tuned through applying vertical compressive strain ϵ . Here, $\epsilon = \frac{r_s - r_0}{r_0} \times 100\%$ and r_s represents the strained interlayer separation. As shown in **Fig. 4(c)**, both ΔE_b^{Max} and ΔE_b^{Min} increase with ϵ , reflecting the enhanced strength of the interlayer coupling energy. We then investigate the influence of ϵ on spin textures in twist bilayer NiBr₂ at $\theta = 2.450^\circ$, as shown in **Figs. 4(d)** and **S10** [45]. Interestingly, at $\epsilon = 5\%$, twist bilayer NiBr₂ exhibits a coexistence of meron–antimeron loops and in-plane textures, indicating the emergence of twist-tunable topological magnetism. To confirm it, we explore the evolution of spin textures in strain twisted bilayer NiBr₂ with twist angle θ . With increasing θ up to 5.360° , as shown in **Fig. 4(d)**, merons and antimerons pair up into bimerons, accompanied by the appearance of high-order merons, thereby establishing the twist tunable moiré topological magnetism in strained twisted bilayer NiBr₂.

Conclusions

In summary, we establish a universal, field-free approach to generate and control moiré topological magnetism in 2D systems originally hosting trivial spin spirals. The frustration between twist-induced FM/AFM domains and uniform AFM interlayer exchange spontaneously stabilizes diverse topological magnetic phases, controlled purely by twist angle. First-principles and spin-

model calculations reveal twist tunable isolated AFM bimerons, merons, antimerons, and high-order magnetic quasiparticles in NiCl₂, in contrast to trivial AFM spin-spiral textures in NiBr₂. These trivial spin spirals, however, can be transformed into intriguing topological magnetism through applying vertical compressive strain. Overall, this work establishes a new foundational platform to topological spintronics where topologically non-trivial spin textures can be generated from their trivial counterparts by 2D twist engineering.

Conflict of Interest

The authors declare no competing financial interest.

Acknowledgements

This work was supported by the National Natural Science Foundation of China (No. 12274261) and Taishan Young Scholar Program of Shandong Province. The research at University of Nebraska was supported by the National Science Foundation through the EPSCoR RII Track-1 program (NSF Grant No. OIA-2044049) and the UNL Grand Challenges catalyst award “Quantum Approaches Addressing Global Threats.”

References

- [1] S. Meyer, M. Perini, S. von Malottki, A. Kubetzka, R. Wiesendanger, K. von Bergmann and S. Heinze, Isolated zero field sub-10 nm skyrmions in ultrathin Co films. *Nat. Commun.* **10**, 3823 (2019).
- [2] B. Göbel, I. Mertig and O. A. Tretiakov, Beyond skyrmions: Review and perspectives of alternative magnetic quasiparticles. *Phys. Rep.* **895**, 1 (2021).
- [3] N. Nagaosa and Y. Tokura, Topological properties and dynamics of magnetic skyrmions. *Nat. Nanotechnol.* **8**, 899 (2013).
- [4] A. Soumyanarayanan, M. Raju, A. L. Gonzalez Oyarce, A. K. Tan, M. Y. Im, A. P. Petrović, P. Ho, K. H. Khoo, M. Tran, C. K. Gan and F. Ernult, Tunable room-temperature magnetic skyrmions in Ir/Fe/Co/Pt multilayers. *Nat. Mater.* **16**, 898 (2017).

- [5] Q. H. Wang, A. Bedoya-Pinto, M. Blei, A. H. Dismukes, A. Hamo, S. Jenkins, M. Koperski, Y. Liu, Q. C. Sun, E. J. Telford and H. H. Kim, The magnetic genome of two-dimensional van der Waals materials. *ACS Nano* **16**, 6960 (2022).
- [6] R. Wiesendanger, Nanoscale magnetic skyrmions in metallic films and multilayers: a new twist for spintronics. *Nat. Rev. Mater.* **1**, 1 (2016).
- [7] T. Kurumaji, T. Nakajima, M. Hirschberger, A. Kikkawa, Y. Yamasaki, H. Sagayama, H. Nakao, Y. Taguchi, T. H. Arima and Y. Tokura, Skyrmion lattice with a giant topological Hall effect in a frustrated triangular-lattice magnet. *Science* **365**, 914 (2019).
- [8] K. Dou, Z. He, J. Zhao, W. Du, Y. Dai, B. Huang and Y. Ma, Engineering topological spin Hall effect in 2D multiferroic material. *Adv. Sci.* **11**, 2407982 (2024).
- [9] Z. He, K. Dou, W. Du, Y. Dai, B. Huang and Y. Ma, Mixed Bloch-Néel type skyrmions in a two-dimensional lattice. *Phys. Rev. B* **109**, 024420 (2024).
- [10] S. Zhang, R. Xu, N. Luo and X. Zou, Two-dimensional magnetic materials: structures, properties and external controls. *Nanoscale* **13**, 1398 (2021).
- [11] B. Huang, G. Clark, E. Navarro-Moratalla, D. R. Klein, R. Cheng, K. L. Seyler, D. Zhong, E. Schmidgall, M. A. McGuire, D. H. Cobden and W. Yao, Layer-dependent ferromagnetism in a van der Waals crystal down to the monolayer limit. *Nature* **54**, 270 (2017).
- [12] Q. Liu, W. Su, Y. Gu, X. Zhang, X. Xia, L. Wang, K. Xiao, N. Zhang, X. Cui, M. Huang and C. Wei, Surprising pressure-induced magnetic transformations from helimagnetic order to antiferromagnetic state in NiI_2 . *Nat. Commun.* **16**, 4221 (2025).
- [13] J. X. Li, W. Q. Li, S. H. Hung, P. L. Chen, Y. C. Yang, T. Y. Chang, P. W. Chiu, H. T. Jeng and C. H. Liu, Electric control of valley polarization in monolayer WSe_2 using a van der Waals magnet. *Nat. Nanotechnol.* **17**, 721 (2022).
- [14] Y. Wu, S. Zhang, J. Zhang, W. Wang, Y. L. Zhu, J. Hu, G. Yin, K. Wong, C. Fang, C. Wan and X. Han, Néel-type skyrmion in $\text{WTe}_2/\text{Fe}_3\text{GeTe}_2$ van der Waals heterostructure. *Nat. Commun.* **11**, 3860 (2020).
- [15] M. Bonilla, S. Kolekar, Y. Ma, H. C. Diaz, V. Kalappattil, R. Das, T. Eggers, H. R. Gutierrez, M. H. Phan and M. Batzill, Strong room-temperature ferromagnetism in VSe_2 monolayers on van der Waals substrates. *Nat. Nanotech.* **13**, 289 (2018).
- [16] D. Ghazaryan, M. T. Greenaway, Z. Wang, V. H. Guarochico-Moreira, I. J. Vera-Marun, J. Yin, Y. Liao, S. V. Morozov, O. Kristanovski, A. I. Lichtenstein and M. I. Katsnelson,

- Magnon-assisted tunnelling in van der Waals heterostructures based on CrBr₃. *Nat. Electron.* **1**, 344 (2018).
- [17] K. Huang, E. Schwartz, D. F. Shao, A. A. Kovalev and E. Y. Tsybal, Magnetic antiskyrmions in two-dimensional van der Waals magnets engineered by layer stacking. *Phys. Rev. B* **109**, 024426 (2024).
- [18] Q. Song, C. A. Occhialini, E. Ergeçen, B. Ilyas, D. Amoroso, P. Barone, J. Kapeghian, K. Watanabe, T. Taniguchi, A. S. Botana and S. Picozzi, Evidence for a single-layer van der Waals multiferroic. *Nature* **602**, 601 (2022).
- [19] J. Sødequist and T. Olsen, Type II multiferroic order in two-dimensional transition metal halides from first principles spin-spiral calculations. *2D Mater.* **10**, 035016 (2023).
- [20] M. A. McGuire, Crystal and magnetic structures in layered, transition metal dihalides and trihalides. *Crystals* **7**, 121 (2017).
- [21] Y. Wang, S. Dong and X. Yao, Frustration-induced magnetic bimerons in transition metal halide CoX₂ (X = Cl, Br) monolayers. *Phys. E* **153**, 115776 (2023).
- [22] H. Y. Yuan, O. Gomonay and M. Kläui, Skyrmions and multisublattice helical states in a frustrated chiral magnet. *Phys. Rev. B* **96**, 134415 (2017).
- [23] D. Amoroso, P. Barone and S. Picozzi, Spontaneous skyrmionic lattice from anisotropic symmetric exchange in a Ni-halide monolayer. *Nat. Commun.* **11**, 5784 (2020).
- [24] J. Cai, E. Anderson, C. Wang, X. Zhang, X. Liu, W. Holtzmann, Y. Zhang, F. Fan, T. Taniguchi, K. Watanabe and Y. Ran, Signatures of fractional quantum anomalous Hall states in twisted MoTe₂. *Nature* **622**, 63 (2023).
- [25] E. Redekop, C. Zhang, H. Park, J. Cai, E. Anderson, O. Sheekey, T. Arp, G. Babikyan, S. Salters, K. Watanabe and T. Taniguchi, Direct magnetic imaging of fractional Chern insulators in twisted MoTe₂. *Nature* **635**, 584 (2024).
- [26] T. I. Andersen, G. Scuri, A. Sushko, K. De Greve, J. Sung, Y. Zhou, D. S. Wild, R. J. Gelly, H. Heo, D. Bérubé and A. Y. Joe, Excitons in a reconstructed moiré potential in twisted WSe₂/WSe₂ homobilayers. *Nat. Mater.* **20**, 480 (2021).
- [27] G. Scuri, T. I. Andersen, Y. Zhou, D. S. Wild, J. Sung, R. J. Gelly, D. Bérubé, H. Heo, L. Shao, A. Y. Joe and A. M. Mier Valdivia, Electrically tunable valley dynamics in twisted WSe₂/WSe₂ bilayers. *Phys. Rev. Lett.* **124**, 217403 (2020).

- [28] K. Hejazi, Z. X. Luo and L. Balents, Noncollinear phases in moiré magnets. *Proc. Natl. Acad. Sci. U.S.A.* **117**, 1072 (2020).
- [29] Q. Tong, F. Liu, J. Xiao and W. Yao, Skyrmions in the moiré of van der Waals 2D magnets. *Nano Lett.* **18**, 719 (2018).
- [30] F. Xiao, K. Chen and Q. Tong, Magnetization textures in twisted bilayer CrX_3 ($X = \text{Br}, \text{I}$). *Phys. Rev. Res.* **3**, 013027 (2021).
- [31] M. Akram, H. LaBollita, D. Dey, J. Kapeghian, O. Erten and A. S. Botana, Moiré skyrmions and chiral magnetic phases in twisted CrX_3 ($X = \text{I}, \text{Br}, \text{and Cl}$) bilayers. *Nano Lett.* **21**, 663 (2021).
- [32] M. Akram, J. Kapeghian, J. Das, R. Valentí, A. S. Botana and O. Erten, Theory of moiré magnetism in twisted bilayer $\alpha\text{-RuCl}_3$. *Nano Lett.* **24**, 89 (2024).
- [33] M. A. Keskiner, P. Ghaemi, M. O. Oktel and O. Erten, Theory of moiré magnetism and multidomain spin textures in twisted Mott insulator–semimetal heterobilayers. *Nano Lett.* **24**, 857 (2024).
- [34] X. Li, C. Xu, B. Liu, X. Li, L. Bellaiche and H. Xiang, Realistic spin model for multiferroic NiI_2 . *Phys. Rev. Lett.* **131**, 036701 (2023).
- [35] T. V. Antão, J. L. Lado and A. O. Fumega, Electric field control of moiré skyrmion phases in twisted multiferroic NiI_2 bilayers. *Nano Lett.* **24**, 15767 (2024).
- [36] H. Zhu, H. Yu, W. Zhu, G. Yu, C. Xu and H. Xiang, Moiré-induced magnetoelectricity in twisted bilayer NiI_2 . *Phys. Rev. Lett.* **135**, 196701 (2025).
- [37] R. Peng, T. Zhang, Z. He, Q. Wu, Y. Dai, B. Huang and Y. Ma, Intrinsic layer-polarized anomalous Hall effect in bilayer MnBi_2Te_4 . *Phys. Rev. B* **107**, 085411 (2023).
- [38] Y. Feng, Y. Dai, B. Huang, L. Kou and Y. Ma, Layer Hall effect in multiferroic two-dimensional materials. *Nano Lett.* **2**, 5367 (2023).
- [39] Y. Zhu, M. Gu, Y. Liu, X. Chen, Y. Li, S. Du and Q. Liu, Sliding ferroelectric control of unconventional magnetism in stacked bilayers. *Phys. Rev. Lett.* **135**, 056801 (2025).
- [40] J. Das, M. Akram and O. Erten, Revival of antibiskyrmionic magnetic phases in bilayer NiI_2 . *Phys. Rev. B* **109**, 104428 (2024).
- [41] T. Okubo, S. Chung and H. Kawamura, Multiple- q states and the skyrmion lattice of the triangular-lattice Heisenberg antiferromagnet under magnetic fields. *Phys. Rev. Lett.* **108**, 017206 (2012).

- [42] D. Ghader, B. Jabakhanji and A. Stroppa, Whirling interlayer fields as a source of stable topological order in moiré CrI₃. *Commun. Phys.* **5**, 192 (2022).
- [43] J. Barker and O. A. Tretiakov, Static and dynamical properties of antiferromagnetic skyrmions in the presence of applied current and temperature. *Phys. Rev. Lett.* **116**, 147203 (2016).
- [44] X. Zhang, J. Xia, L. Shen, M. Ezawa, O. A. Tretiakov, G. Zhao, X. Liu and Y. Zhou, Static and dynamic properties of bimerons in a frustrated ferromagnetic monolayer. *Phys. Rev. B* **101**, 144435 (2020).
- [45] See Supplemental Material for the computational details and supplemental figures, which include Refs. [23, 29, 34-36, 42, 47-60].
- [46] T. Dohi, S. DuttaGupta, S. Fukami and H. Ohno, Formation and current-induced motion of synthetic antiferromagnetic skyrmion bubbles. *Nat. Commun.* **10**, 5153 (2019).
- [47] P. E. Blöchl, Projector augmented-wave method. *Phys. Rev. B* **50**, 17953 (1994).
- [48] G. Kresse and J. Hafner, Ab initio molecular-dynamics simulation of the liquid-metal–amorphous-semiconductor transition in germanium. *Phys. Rev. B* **49**, 14251 (1994).
- [49] G. Kresse and J. Furthmüller, Efficient iterative schemes for ab initio total-energy calculations using a plane-wave basis set. *Phys. Rev. B* **54**, 11169 (1996).
- [50] J. P. Perdew, K. Burke and M. Ernzerhof, Generalized gradient approximation made simple. *Phys. Rev. Lett.* **77**, 3865 (1996).
- [51] S. Grimme, S. Ehrlich and L. Goerigk, Effect of the damping function in dispersion corrected density functional theory. *J. Comput. Chem.* **32**, 1456 (2011).
- [52] A. Rohrbach, J. Hafner and G. Kresse, Electronic correlation effects in transition-metal sulfides. *J. Phys.: Condens. Matter.* **15**, 979 (2003).
- [53] C. Xu, J. Feng, H. Xiang and L. Bellaiche, Interplay between Kitaev interaction and single ion anisotropy in ferromagnetic CrI₃ and CrGeTe₃ monolayers. *npj Comput. Mater.* **4**, 57 (2018).
- [54] A. A. Thiele, Steady-state motion of magnetic domains. *Phys. Rev. Lett.* **30**, 230 (1973).
- [55] B. Berg and M. Lüscher, Definition and statistical distributions of a topological number in the lattice O(3) σ -model. *Nucl. Phys. B* **190**, 412 (1981).

- [56] S. H. Sung, Y. M. Goh, H. Yoo, R. Engelke, H. Xie, K. Zhang, Z. Li, A. Ye, P. B. Deotare, E. B. Tadmor and A. J. Mannix, Torsional periodic lattice distortions and diffraction of twisted 2D materials. *Nat. Commun.* **13**, 7826 (2022).
- [57] C. Xu, P. Chen, H. Tan, Y. Yang, H. Xiang and L. Bellaiche, Electric-field switching of magnetic topological charge in type-I multiferroics. *Phys. Rev. Lett.* **125**, 037203 (2020).
- [58] Q. Cui, Y. Zhu, Y. Ga, J. Liang, P. Li, D. Yu, P. Cui and H. Yang, Anisotropic Dzyaloshinskii-Moriya interaction and topological magnetism in two-dimensional magnets protected by $P\bar{4}m2$ crystal symmetry. *Nano Lett.* **22**, 2334 (2022).
- [59] Y. Ga, Q. Cui, Y. Zhu, D. Yu, L. Wang, J. Liang and H. Yang, Anisotropic Dzyaloshinskii-Moriya interaction protected by D_{2d} crystal symmetry in two-dimensional ternary compounds. *npj Comput. Mater.* **8**, 128 (2022).
- [60] V. Lohani, C. Hickey, J. Masell and A. Rosch, Quantum skyrmions in frustrated ferromagnets. *Phys. Rev. X* **9**, 041063 (2019).